New Experimental Limit on the Electron Electric Dipole Moment

K. Abdullah,[1],[2],[a] C. Carlberg,[1],[b] E. D. Commins,[1],[2] Harvey Gould,[1],[c] and Stephen B. Ross[1],[2],[d]

[1]*Chemical Sciences Division, Building 71-259, Lawrence Berkeley Laboratory, One Cyclotron Road, Berkeley, California 94720*

[2]*Department of Physics, University of California, Berkeley, California 94720*

(Received 31 August 1990)

A search for the electron electric dipole moment d_e is carried out with two counterpropagating beams of ground-state ^{205}Tl. The experiment employs atomic-beam magnetic resonance with separated oscillatory fields combined with laser state selection and fluorescence detection. Extensive tests were made for possible systematic effects. The result for the atomic electric dipole moment is $d_a = (1.6 \pm 5.0) \times 10^{-24}$ e cm, where the uncertainty includes equal statistical and systematic contributions. This yields $d_e = (-2.7 \pm 8.3) \times 10^{-27}$ e cm, assuming the ratio $d_a/d_e = -600$.

PACS numbers: 13.40.Fn, 11.30.Er, 14.60.Cd, 35.10.Wb

We have made a new search for the electron electric dipole moment (EDM), which can exist only if parity (P) and time-reversal invariance (T) are violated. In the standard model, where CP violation (equivalent to T violation) arises from the Kobayashi-Maskawa matrix,[1] the electron EDM d_e is predicted to be no larger than 10^{-37} e cm. However, other models of CP violation predict values for d_e of experimental interest;[2] in particular, it has recently been shown that Higgs-boson models[3] of CP violation can yield values of $d_e > 10^{-27}$ e cm.

The principle of our experiment is to search for d_e by measuring its energy in an electric field. While this is impractical for the free electron, it is feasible using a valence electron in a $J = \frac{1}{2}$ neutral atom of high Z, where, due to relativistic effects, the ratio R of the atomic EDM (d_a) to d_e is much larger than unity.[4] We use the $6\,^2P_{1/2}$ ground state of ^{205}Tl ($Z = 81$) where R is estimated[5] to be -600, and search for d_a by looking for an energy splitting ΔW, linear in an applied electric field E_z, between the $m_F = \pm 1$ components of the $6\,^2P_{1/2}$, $F = 1$ state.

Systematic contributions to ΔW can arise from the interaction of the large atomic magnetic moment with any magnetic field that reverses with E_z. A motional magnetic field $\mathbf{B}_{\rm mot} = \mathbf{E} \times \mathbf{v}/c$, where $\mathbf{v}$ is the atomic velocity, causes a splitting $\Delta W_{\rm mot}$ that reverses with E_z if any applied magnetic field $\mathbf{B}$ is not exactly parallel to E_z. However, $\Delta W_{\rm mot}$ reverses with $\mathbf{v}$; hence this effect is almost completely eliminated by using a pair of counterpropagating atomic beams with opposite velocities.

Counterpropagating beams are generated in resistively heated ovens (see Fig. 1) and propagate in vacuum with most-probable speeds $\approx 4.3 \times 10^4$ cm/s. We follow the up beam, which intersects a cw laser beam, directed along y and with linear polarization along z, in the state selector region. The entire experiment from here on takes place in a nominally uniform magnetic field B_z, typically 0.26 G or less, in the z direction. The laser is tuned to the transition $6\,^2P_{1/2}(F=1) \rightarrow 7\,^2S_{1/2}(F=1)$ at 378 nm in ^{205}Tl (see Fig. 2). Only $6\,^2P_{1/2}$ atoms with $m_F = \pm 1$ make this transition because the Clebsch-Gordan coefficient $\langle 1,0,1,0|1,0\rangle$ is zero. Once excited, the atoms decay back to the $6\,^2P_{1/2}$ state, or to the $6\,^2P_{3/2}$ state with fluorescence at 535 nm (branching ra-

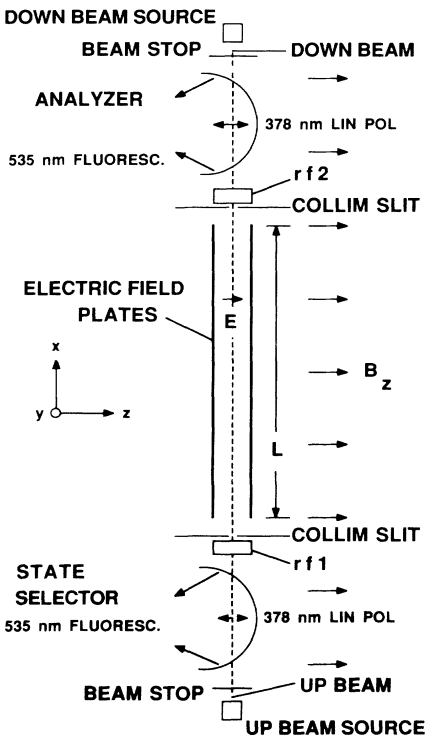

FIG. 1. Schematic diagram of the apparatus. The 378-nm laser beams are perpendicular to the page. Magnetic fields are produced in the z and y directions by rectangular coils, and in the x direction by circular coils. The magnetic-field region is surrounded by four concentric cylindrical magnetic shields with end caps to reduce external fields. The entire apparatus is vertical as shown. If it were horizontal, gravity would affect the collinearity or velocity match of the two beams.

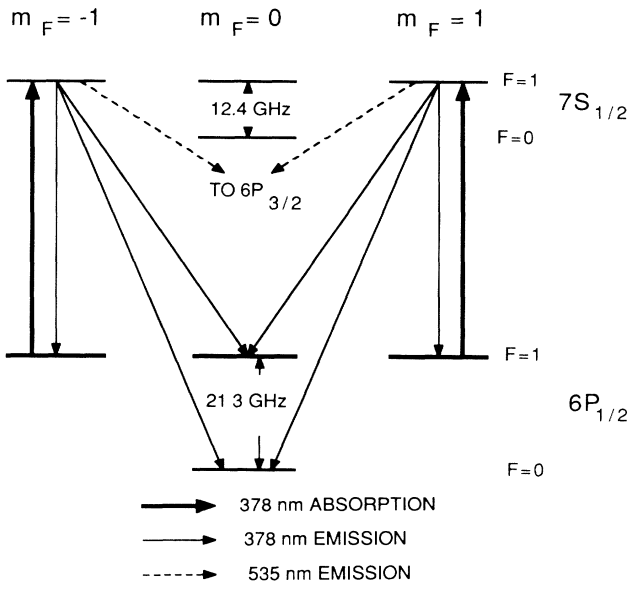

FIG. 2. Energy-level diagram (not to scale) showing the state selection scheme.

tio $\approx 50\%$). The lifetime of the latter state is long compared to the transit time of the beam through the apparatus. Hence the ground-state components $F=1$, $m_F = \pm 1$ are depopulated and, as $F=1$ atoms leave the state selector, they are in the state $m_F = 0$

Further along the up-beam trajectory is a second laser intersection region called the analyzer. (The analyzer for the up beam serves as the state selector for the down beam and vice versa.) Here, the atomic beam intersects a beam from the same laser, again directed along y with linear polarization along z, and tuned to the same transition $6P_{1/2}(F=1) \rightarrow 7S_{1/2}(F=1)$. The analyzer fluorescence at 535 nm is our signal (S), and is proportional to the sum of the populations of $F=1$, $m_F = \pm 1$ atoms that enter this region. S is nonzero only if reorientation of the $F=1$ state occurs in the intermediate space (because of rf and electric fields). Intersections between the laser and atomic beams in the state selector and analyzer occur at the foci of ellipsoidal mirrors with axes of revolution along z. Their purpose is to collect 535-nm fluorescence and focus it through a light pipe-optical filter system into a photomultiplier tube.

In the region between state selector and analyzer, transitions between $F=1$, $m_F=0$ and $m_F = \pm 1$ are induced by oscillatory magnetic fields[6] rf1 and rf2, each 5 cm long, directed along the x axis and separated by $L_{\rm rf}=120$ cm. The applied frequency $\nu=\omega/2\pi$ is set to the transition frequency $\nu_0=\omega_0/2\pi$ to within 1 Hz. The transition frequency, determined by B_z, is typically 120 kHz or less. The resonance FWHM, determined by the beam transit time, is 45 Hz. rf2 leads rf1 by a phase ϕ, which is $\pm\pi/4$ or $\pm 3\pi/4$, so that $|\partial S/\partial\omega|$ is a maximum on resonance. The phase ϕ is changed every 68 ms, in order to reduce noise due to atomic- and laser-beam fluctuations.

In the region between rf1 and rf2 a pair of parallel titanium alloy plates of length $L_E = 100$ cm and separation 0.2 cm is used to generate E_z, typically 110 kV/cm. The electric field is reversed every 0.93 s. Also data are taken with one beam at a time and we switch between them every 7.4 s. In order to calibrate the sensitivity to d_a we measure the signal difference as ν is shifted by 1 Hz above and below ν_0 every 3.7 s. After 128 beam-reversal periods have elapsed, an average EDM and its standard deviation are calculated. This result is a data point, which represents about 70 min of real time. Our data points are shown in Figs. 3(a) and 3(b). After each such point, all magnetic coil currents are reversed and/or the E plate cables are reversed manually, to distinguish between an EDM asymmetry and asymmetries due to systematics which are even under E and/or B.

It may be shown that near resonance, for a single beam velocity, and for optimum rf power, the analyzer signal would be proportional to

$$S = 1 + \lambda\left(2\Delta\omega\frac{L_{\rm rf}}{v} \mp \frac{\Delta W_{\rm EDM}L_E}{\hbar v} \mp \frac{\Delta W_{\rm syst}L_E}{\hbar v}\right), \qquad (1)$$

where $\Delta\omega = \omega - \omega_0$, the $-$ $(+)$ sign is employed for $B_z > 0$ ($B_z < 0$), $\Delta W_{\rm EDM} = -2d_aE_z$ is the energy splitting between $m_F = \pm 1$ states due to d_a, and $\Delta W_{\rm syst}$ is the splitting arising from systematic effects. Also $\lambda = +1$ for $\phi = \pi/4$ or $-3\pi/4$, and $\lambda = -1$ for $\phi = -\pi/4$ or $3\pi/4$ for the up beam, while the sign of λ is reversed for the down beam. As is evident from (1), S contains an asymmetry proportional to the P,T-odd rotational invariant $\mathbf{E}\cdot\mathbf{B}$ if $\Delta W_{\rm EDM} \neq 0$. In reality one must take into

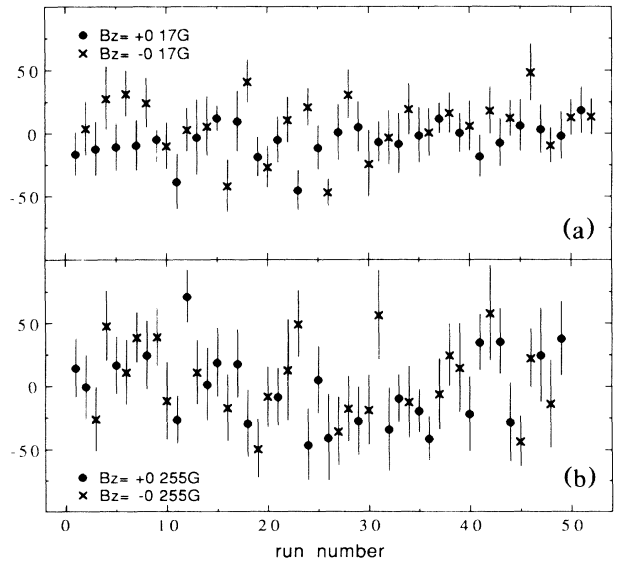

FIG. 3. Data points for (a) run 1, (b) run 2, with vertical axis in units of 10^{-24} e cm. In each graph, the signs of d_a for all $-B$ data points are reversed, for comparison with $+B$ data points. Error bars represent standard error in the mean.

account various features not contained in the simplified formula (1), such as the beam velocity distribution and a quadratic Stark shift between the $m_F=0$ and $m_F=\pm 1$ components.

We briefly describe important sources of systematic error (see Table I) and steps taken to minimize them. While the $B_{\rm mot}$ *systematic* effect is largely eliminated by use of counterpropagating beams, the following residual remains:

$$\Delta W_{\rm mot}=\text{const}\times\{(\bar{v}_y\langle B_x/B_z\rangle-\bar{v}_x\langle B_y/B_z\rangle)_{\rm up} + (\bar{v}_y\langle B_x/B_z\rangle-\bar{v}_x\langle B_y/B_z\rangle)_{\rm down}\}\,, \quad (2)$$

where the velocities are averaged over the velocity distribution, $B_{x,y,z}$ are the magnetic-field components, and $\langle\cdots\rangle$ indicates an average over L_E. Let $\bar{v}_{x,y\,\rm up}=\bar{v}_{x,y\,\rm down}+\delta\bar{v}_{x,y}$ and $\langle B_{x,y}/B_z\rangle_{\rm up}=\langle B_{x,y}/B_z\rangle_{\rm down}+\delta B_{x,y}/B_z$, with $|v_x|\gg|v_y|$ and $|B_z|\gg|B_{x,y}|$. Inserting these expressions into (2) and dropping second order and very small terms, we obtain

$$\Delta W_{\rm mot}=\text{const}\times(\delta\bar{v}_y\langle B_x/B_z\rangle-\delta\bar{v}_x\langle B_y/B_z\rangle+\bar{v}_x\delta B_y/\langle B_z\rangle)\,. \quad (3)$$

We minimize $\delta\bar{v}_y\langle B_x/B_z\rangle$ by employing auxiliary x coils to cancel any residual B_x. The quantity $\langle B_x/B_z\rangle$ is measured by applying a known B_x and observing the change in resonance frequency on its reversal. In the second term of (3), $\delta\bar{v}_x$ is minimized by comparing the resonance widths of the up and down beams and adjusting the oven temperatures to equalize these widths to within 1%. We continuously measure $\langle B_y/B_z\rangle$ by comparing up- and down-beam asymmetries and maintain $\langle B_y/B_z\rangle$ at less than 1×10^{-5} on the average. The third term of (3) is nonzero if both beams do not experience the same B_y. This is possible if the two beams do not overlap exactly in y and z and if the magnetic field is inhomogeneous. Two methods are used to measure this contribution. In the first, a large magnetic-field gradient is imposed, and we measure the EDM asymmetry and minimize it by adjusting the oven positions. In the second, the residual magnetic-field inhomogeneity is determined by measuring resonant frequency shifts as we scan either atomic beam over y and z. The beam overlap is determined by measuring the difference in the resonant frequencies of up and down beams when large external magnetic-field gradients are imposed. The two methods give consistent results.

TABLE I. Contributions to the uncertainty in d_a (10^{-24} e cm).

Contribution	Run 1 $B_z=0.17$ G	Run 2 $B_z=0.255$ G
E×v		
Nonzero v_y and B_x	3.5	1.2
Velocity difference and residual B_y	0.3	0.3
Imperfect overlap and field gradients	3.3	0.4
Geometrical phase effect	2.4	1.0
Discharge currents	0.4	0.8
Charging currents	0.4	0.4
Total systematic uncertainty[a]	5.4	1.9
Statistical uncertainty	2.5	4.6

[a]Calculated by combining individual contributions in quadrature.

A *geometric phase* effect arises when a magnetic field B_x exists with different values at the two ends of the electric-field region x_1,x_2, and where the magnetic moment precesses many times in the lengths over which E varies between zero and its full value.[7] For $|B_z|\gg|B_x|$, $|vE_z/c|$, the $m_F=\pm1$ components suffer equal and opposite phase shifts $v_xE_z(B_{x1}-B_{x2})/cB_z^2$, with the same sign for both beams, a result verified experimentally by deliberately imposing a large x-field gradient. If $B_{x1}-B_{x2}$ reverses when the current to the magnetic-field coils reverses, the resulting asymmetry is E odd but B even and thus distinguishable from an EDM asymmetry. A small B-even effect is seen in our data (see below and Fig. 3). An x-field gradient that does not reverse with current may arise from leakage of external magnetic fields through our shielding. This would cause a systematic which scales with B_z^{-2}. The results of measurements made at $B_z=0.085$ G to set an upper limit to this effect are included in our systematic uncertainty in Table I.

Magnetic fields, synchronous with the electric field, could occur because of discharges across the electric-field plates or to ground. The current flowing to the plates is monitored and E_z chosen to keep the discharge current below 10^{-8} A. We test for the effect of discharge currents by taking EDM data with larger E_z, where the discharge currents are $\approx10^{-6}$ A.

We have also calculated and/or tested for possible systematic effects due to charging currents, incomplete E reversal, phase-shift errors and amplitude differences between rf1 and rf2, quadratic Stark shifts, differences in B_z at and between rf1 and rf2, different velocity distributions and backgrounds for the two beams, gravitational acceleration of the beams, calibration errors, ground loops, and insufficient delays after reversals and before restarting data collection. Among these, only contributions due to charging currents are significant at our present level of sensitivity (and are included in Table I).

Except for infrequent automatic rejection based on excessive noise, no rejections or cuts were made nor were any corrections applied to our EDM data. There were two separate runs. Run 1, done at $B_z=0.17$ G, resulted in 51 data points [Fig. 3(a)]. It yielded $d_a=[1.1\pm2.5(\text{stat})\pm5.4(\text{syst})]\times10^{-24}$ e cm with the statistical uncertainty here as elsewhere at 68% confidence interval. The systematic uncertainty was dominated by contribu-

tions due to $\mathbf{B}_{\text{mot}}$ and geometric phase effects. In run 2 the uncertainties due to these effects were reduced, in the latter case by taking data at $B_z = 0.255$ G. However, the noise was larger and the sensitivity to a possible EDM was decreased because we employed an electric field of 100 kV/cm, rather than 112 kV/cm, as in run 1. With 49 data points, run 2 resulted in $d_a = [2.1 \pm 4.6(\text{stat}) \pm 1.9(\text{syst})] \times 10^{-24}$ e cm, in agreement with the result from run 1. We did a test run at $B_z = 0.085$ G to put a limit on the B-odd geometric phase effect and to determine the magnetic-field dependence of any other systematic asymmetry. All the data taken at the three values of B_z are consistent with a B-even asymmetry proportional to B_z^{-2}. We find no evidence for any effect that is both B odd and E odd. We combine the statistical and systematic uncertainties in each run, and taking the resulting weighted average of the two runs we obtain $d_a = (1.6 \pm 5.0) \times 10^{-24}$ e cm. Assuming $R = -600$, this gives $d_e = (-2.7 \pm 8.3) \times 10^{-27}$ e cm, where the theoretical uncertainty in R is not included. This yields a limit on d_e at least a factor of 7 smaller than that obtained from all previous measurements.[8,9]

We thank Alex Vaynberg for outstanding machining, Douglas McColm for his contributions to the experiment, Nelson Claytor and Narasimhan Larkin for assistance in assembling the apparatus, Alfred Wydler for assistance with electronics, and Edward Garwin, Klaus Halbach, Donald Hopkins, Iosif Khriplovich, Walter Johnson, and Mahiko Suzuki for useful discussions. This work was supported by the U.S. Department of Energy under Contract No. DE-AC03-76SF00098, through the Lawrence Berkeley Laboratory's Exploratory Research and Development Fund Program; and by the Director, Office of Energy Research, Office of Basic Energy Sciences, Chemical Sciences Division; and in part by the Office of High Energy and Nuclear Physics, Division of High Energy Physics and Division of Nuclear Physics.

[a]Present address: Salomon Brothers Inc., 1 New York Plaza, New York, NY 10004.

[b]Present address: Manne Siegbahn Institute of Physics, Frescativ 24, 104 05, Stockholm, Sweden. Electronic address: carlberg@sesuf51.bitnet.

[c]Electronic address: gould@lbl.bitnet.

[d]Electronic address: stephen@ux5.lbl.gov.

[1]For reviews of this subject, see, for example, S. M. Barr and W. J. Marciano, in *CP Violation*, edited by C. Jarlskrog (World Scientific, Singapore, 1989), p. 455; W. Bernreuther and M. Suzuki, Lawrence Berkeley Laboratory Report No. LBL-27985, 1990 (to be published).

[2]S. M. Barr and A. Masiero, Phys. Rev. Lett. **58**, 187 (1987).

[3]S. M. Barr and A. Zee, Phys. Rev. Lett. **65**, 21 (1990); R. G. Leigh, S. Paban, and R. M. Xu, University of Texas Theory Group Report No. 27-90, 1990 (unpublished).

[4]P. G. H. Sandars, Phys. Lett. **14**, 194 (1965).

[5]P. G. H. Sandars and R. M. Sternheimer, Phys. Rev. A **11**, 473 (1975); V. V. Flambaum, Yad. Fiz. **24**, 383 (1976) [Sov. J. Nucl. Phys. **24**, 199 (1976)]; W. R. Johnson, D. S. Guo, M. Idrees, and J. Saperstein, Phys. Rev. A **32**, 2093 (1985); **34**, 1043 (1986); E. Lindroth, A. M. Martensson-Pendrill, A. Ynnerman, and P. Oster, J. Phys. B **22**, 2447 (1989); A. C. Hartley and P. G. H. Sandars (private communication).

[6]N. F. Ramsey, Phys. Rev. **76**, 996 (1949); Science **248**, 1612 (1990).

[7]M. V. Berry, Proc. Roy. Soc. London, A **392**, 45 (1984).

[8]S. A. Murthy, D. Krause, Jr., Z. L. Li, and L. R. Hunter, Phys. Rev. Lett. **63**, 965 (1989).

[9]D. Cho, K. Sangster, and E. A. Hinds, Phys. Rev. Lett. **63**, 2559 (1989); S. K. Lamoreaux, J. P. Jacobs, B. R. Heckel, F. J. Raab, and N. Fortson, Phys. Rev. Lett. **59**, 2275 (1987); M. A. Player and P. G. H. Sandars, J. Phys. B **3**, 1620 (1970); H. Gould, Phys. Rev. Lett. **24**, 1091 (1970); M. C. Weisskopf, J. P. Carrico, H. Gould, E. Lipworth, and T. S. Stein, Phys. Rev. Lett. **21**, 1645 (1968).